SEMARAK ILMU PUBLISHING

Journal of Advanced Research in Applied Mechanics

Journal homepage:
https://semarakilmu.com.my/journals/index.php/appl_mech/index
ISSN: 2289-7895

Numerical Simulation of Surface Pressure of a Wedge at Supersonic Mach Numbers and Application of Design of Experiments

Shamitha[1], Asha Crasta[1], Khizar Ahmed Pathan[2], Sher Afghan Khan[3,*]

[1] Department of Mathematics, M.I.T.E, Moodabidri & Affiliated To VTU, Belgavi, Karnataka, India
[2] Department of Mechanical Engineering, Trinity College of Engineering and Research, Pune, India
[3] Department of Mechanical Engineering, Faculty of Engineering, IIUM, Gombak Campus, Kuala Lumpur, Malaysia

ARTICLE INFO

Article history:
Received 1 November 2022
Received in revised form 10 January 2023
Accepted 13 January 2023
Available online 31 January 2023

Keywords:
CFD analysis; supersonic; wedge angle

ABSTRACT

This paper aims to numerically simulate the flow field for wedge, cone, and ogives. Usually, wedge shapes are used as a stabilizing surface for supersonic projectiles like rockets, missiles, and planes in defense applications. Wedge-shaped or delta wings are often the principal wing used for the stability of supersonic aircraft/missiles. The main goal of the current study is to estimate the pressure at the wedge-shaped plane's/missiles nose at different Mach numbers and incidence angles. Analytical pressure distribution is determined using the strip and piston theory. Later the outcomes from the numerical simulations are compared with the results obtained analytically. The analytical and CFD findings matching is very good. The findings demonstrate that the Mach number and wedge angle are the variables that influence the deviation of static pressure. The static pressure on the surface of the wedge grows with the rise in the semi-vertex angle of the wedge angle and the Mach number. This increase in the surface pressure ratio is linear for the increase in Mach number as well as the semi-vertex angle of the wedge. However, the magnitude of increase with the Mach numbers is not the same as what it was for low Mach numbers. The enhancement in the pressure decreases with the Mach numbers.

1. Introduction

Due to rapid growth in the area of high-speed aerodynamics, the majority of the researchers are focusing on supersonic and hypersonic aerodynamics. Because of the prevailing situation in the world who so ever has missiles and fighter planes at large Mach numbers will have air superiority over the others. This is what exactly is seen in the current Ukrain-Russia conflict. Russia has superiority over other countries due to S-400, S-500, and S-600 missile defense systems. Russian fighter planes also have supremacy over others in terms of high Mach number operating conditions. Hence, there is a need to find simple and cost-effective methods to compute the aerodynamic derivatives to simulate the trajectory of the missile systems. As we all know that wind-tunnel testing is a very costly affair

* *Corresponding author.*
E-mail address: sakhan@iium.edu.my

https://doi.org/10.37934/aram.101.1.118

hence researchers are looking for methods to generate stability derivatives for simple shapes like cones and ogives.

Hui explored and developed the exact solution for the oscillating wedge of 2D flow [1]. Lui and Hui extended Hui's 1971 theory for oscillating flat plate delta wings in pitch with connected shock waves [2]. He then determined the solutions for all supersonic Mach values and angles of attack while taking into consideration the associated shock wave. Hui conducted research, produced the precise solution in an oscillating wedge for a 2D flow, and obtained the solutions for all supersonic Mach numbers and angles of attack while taking the associated shock wave for an oscillating flat plate into consideration [2]. Hui's notion of oscillating flat plate delta wings in pitch with associated shock was continued by Lui and Hui. The relationship between the piston hypothesis for the order of two first forward in 1953 by Lighthill and Mile and in 1980 by Ghosh and Mistry. Normally, if a shock wave is attached, the shock's angle with the plane corresponds to the windward surface. For the applicability of their theory, the Mach number behind the shock wave must be greater than or equal to 2.5. In hypersonic flow, Ghosh found a similarity for delta wings with an associated leading edge shock at a considerably large angle of incidence [5]. Ghosh and Mistry [4] linked the ideas of Lighthill [3] with Mile's piston theory for orders of two and higher. Assuming the shock wave is attached, this angle is between the plane that roughly corresponds to the windward surface and the shock. Kalimuthu *et al*., [6] investigated the aerodynamic coefficients of blunt bodies with and without spikes at a speed of Mach number 6. Khan et.al has studied the shape of human-powered submarines and supersonic flow over a 2D wedge [7]-[10]. Pathan *et al*.,[11] have studied boat-tailed helmets to reduce drag using CFD analysis.

Because of the above literature review, there is a need to find the stability derivatives at supersonic Mach numbers by analytical methods. It can arrive at probable geometry for the CFD analysis. Based on the CFD and analytical methods the limited wind tunnel tests can be finalized to arrive at the optimum aerodynamic shape. It is accomplished by calculating various flow parameters for the planar wedge, the current investigation aims to assess the analytical solutions of pressure ratio variation with Mach numbers and wedge angles. The wedge's angle, which ranges from 5 to 25 degrees, is employed. The analytical results are compared in combination with the CFD study. Figure 1 shows the geometry of a plane wedge.

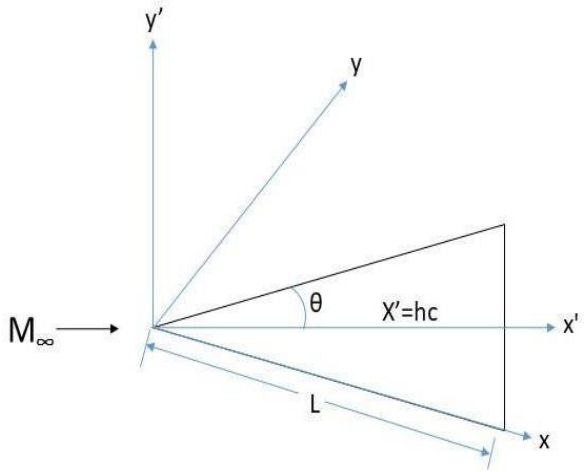

Fig. 1. Geometry of a plane wedge to move the pivot from x_0 to x'_0

Consider the L-length flat plate aerofoil with mean wedge angle θ, which oscillates in pitch with a low amplitude about the O_1 pivot position and is distanced x_0 from its apex. The angle of attack is

α at all times. The minute piston velocity at location x is represented using Eq. (1) and the piston Mach number is given by equation (2).

$$U_P = U_\infty sin\alpha + q(x - x_0) \quad (1)$$

$$M_P = M_\infty \sin\alpha + \frac{q(x-x0)}{a_\infty} \quad (2)$$

where $M_P =$ Piston Mach number
M∞ =Free stream Mach number
α is the angle of attack
q is the pitch rate
a∞ is free stream velocity

Due to the small velocity component in the z-direction, the strip of the wedge parallel to the center line can be taken to be independent along the flow direction. Ghosh has assumed this in his work [5]. The "piston analogy" combines the strip theory with the significant incidence similitude of Ghosh's work and enables surface pressure P to be directly connected with the appropriate Mach number Mp'. In the current situation, the flow deflection angle and piston Mach number "Mp" are considerable.

Accordingly, instead of using the powerful shock piston ideas proposed by Lighthill or Miles, the Ghosh piston hypothesis is used. The surface pressure P can have a direct impact on the amount of inertia at the piston Mp on the wing surface. The expression for pressure distribution is provided by Eq (3).

$$\frac{P_2}{P_1} = 1 + A(M_P)^2 + AM_P\sqrt{B + (M_P)^2} \quad (3)$$

where P_2 is pressure on the windward surface and P_1is free stream pressure

At various span points, strips are thought of as being independent of one another. The wing angle and the wedge angle are the same. 'Mp' is allowed to be high, as is flow deflection in the current situation. The piston theory considered in Eq. (3) can be used to describe supersonic flow as well, and the equation is now denoted by Eq. (4).

$$\frac{P_2}{P_1} = 1 + A\left(\frac{M_P}{cos\emptyset}\right)^2 + A\left(\frac{M_P}{cos\emptyset}\right)\sqrt{B + \left(\frac{M_P}{cos\emptyset}\right)^2} \quad (4)$$

where Ø is the angle between the wing strip and the shock

$$A = \frac{\gamma+1}{4}$$

$$B = \left(\frac{4}{\gamma+1}\right)^2$$

2. CFD analysis

To verify and validate the conclusions of the analytical work, a computational fluid dynamics (CFD) analysis was performed using ANSYS Workbench and Fluent. The analysis takes into account the Mach numbers 1.3, 1.8, 2.3, 2.8, 3.3, 3.8, 4.3, and the wedge angles of 5, 10, 15, 20, and 25

degrees. For CFD analysis, all potential parameter combinations for weak solutions are taken into account to ensure that the shock waves are attached. Air as an ideal gas is used as the fluid in the CFD analysis.

2.1 Modeling

The wedge angle is adjusted in the ANSYS design modeler to model all geometries. The geometry for the 2D wedge and enclosure is shown in figure 2. All geometries are represented by accounting for the various wedge angles (θ), ranging from 5° to 25°. The length (L) = 10 mm is taken into consideration for all models. For CFD analysis, a container with three times the length (L) on the front side, five times the length (L) on the back side, and five times the length (L) on the top and bottom sides is produced. According to Fig. 2, the front and back edges are given the names of the inlet and outflow.

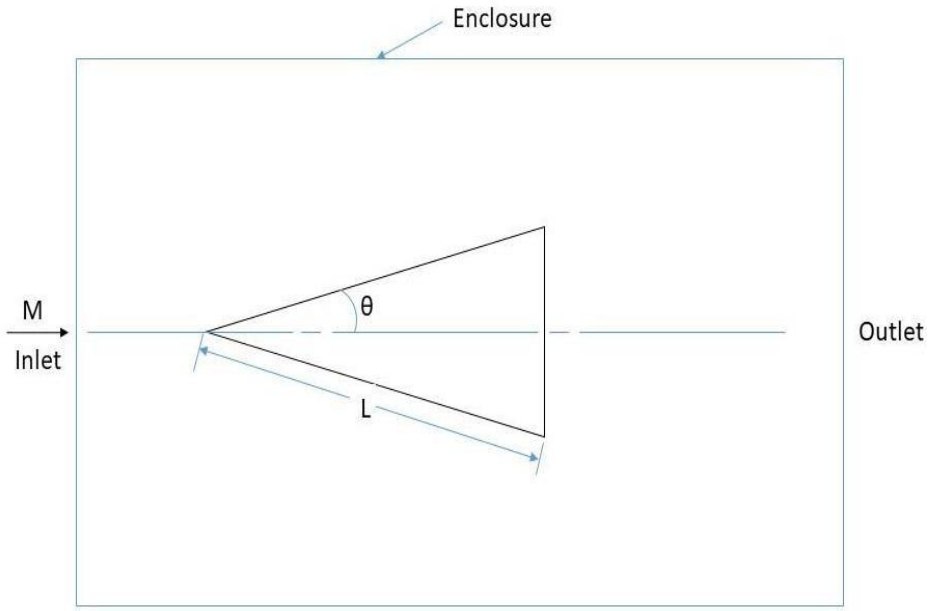

Fig.2. 2D Wedge and enclosure geometry

2.2 Meshing

The grid independence test must be run before finalizing the mesh size to determine the optimal mesh element size. The grid independence test has been run with mesh sizes ranging from 1 mm to 10 mm for Mach number 4.3 and 15° wedge angle. Table 1 displays the number of elements and nodes for mesh sizes ranging from 10 mm to 1 mm.

Table 1
Grid independence test: Number of mesh elements with various element sizes

Mesh Element Size (mm)	No. of Mesh Nodes	No. of Mesh Elements
10	11215	10920
9	13555	13236
8	16544	16199
7	20864	20486
6	27810	27388
5	39355	38870
4	60600	60013
3	106716	105967
2	237306	236239
1	942995	940928

Figure 3 displays the results of the grid independence test. The results clearly show that the outcome is stable for a mesh element size of 7 mm, and the mesh element size of 7 mm can be taken into account for the CFD study. A mesh element size of 04 mm is employed for improved precision in subsequent CFD studies.

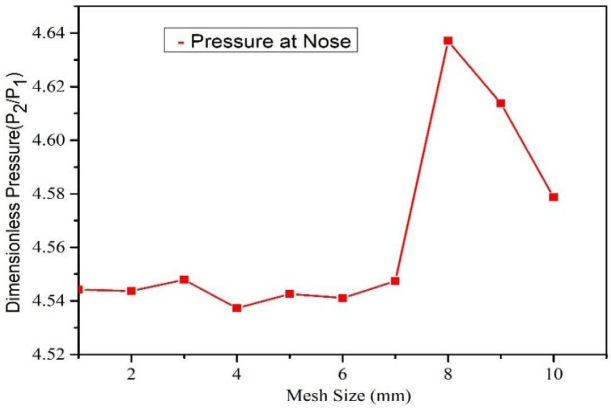

Fig. 3. Grid independence test

The Hexahedral mesh elements are used in the meshing. Figure 4 (a) shows the complete meshed model, and Figure 4(b) shows the enlarged view of the wedge geometry.

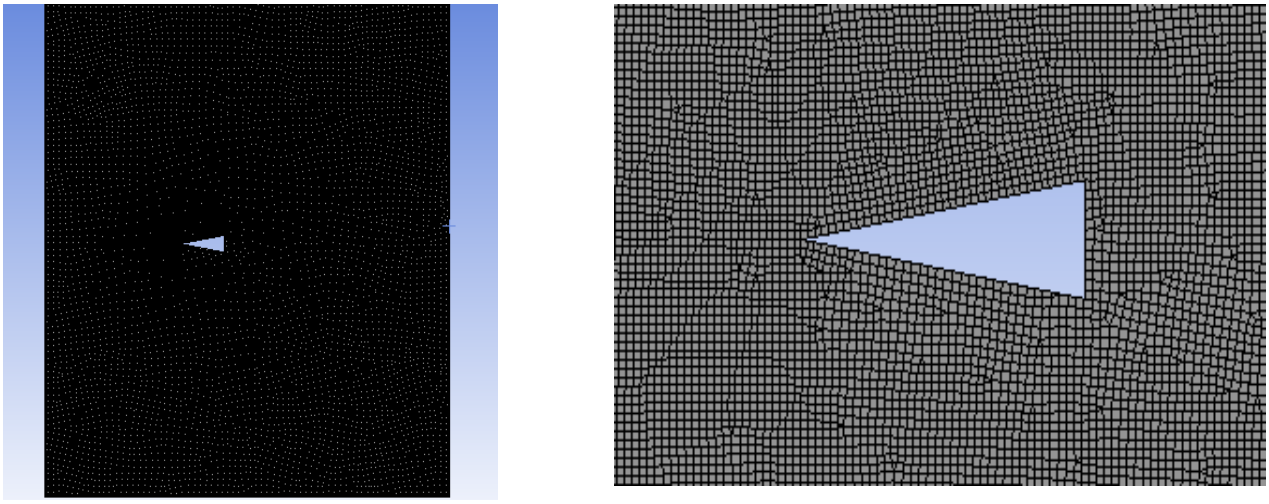

(a) Complete geometry (b) Enlarged view of the wedge

Fig. 4. 2D meshed geometry for Θ=15°and mesh element size 4 mm

2.3 CFD Analysis

For every conceivable set of parameter combinations, the CFD analysis is performed. The k-epsilon turbulent model is used in the analysis as it more reliable and gives accurate results for a variety of boundary conditions [12] - [24]. The terms "velocity inlet" and "pressure outlet" are used to define inlet and outflow boundary conditions respectively. According to Pathan *et al*., [11] boat tail helmets can reduce drag. The solution is initialized, the boundary conditions are established, and at least 10,000 iterations. The answer seems to have converged in several instances after 1000 iterations.

3. Results and Discussion

According to the findings, the Mach cone angle decreases as the Mach number rises while maintaining the same wedge angle. The Mach cone angle (μ) is the same as in cases where the shock is exceedingly weak. Theoretically, the equation provides the Mach cone angle (μ) using equation (4). Additionally, the Mach angle increases as the angle of incidence do. Equation (5) describes the relationship between the angle of incidence (θ), shock angle (β), and Mach number (M).

$$\mu = sin^{-1}\left(\frac{1}{M}\right) \tag{4}$$

$$tan\theta = 2cot\beta\left(\frac{M_1^2\, sin_\beta^2 - 1}{M_1^2\,(\gamma + cos2\beta + 2)}\right) \tag{5}$$

3.1 Main effects plot for dimensionless static pressure

The major effect map for dimensionless static pressure at the wedge's nose is shown in Fig. 5. The mean values of pressure for all cases are considered and plotted in Fig. 5. According to the results, as the Mach number increases, so does the static pressure at the nose due to the increase in the inertia values and hence strength of the oblique shock wave. A progressive increase in the pressure

ratio is observed. It is well known that the pressure ratio after and before the shock wave is a measure indicating the strength of the shock wave located at the nose. Across the shock waves, the stagnation pressure and temperature before and after the shock waves are identical. From the main effects plot, it is seen that the pressure ratio at Mach 2.3, 2.8, 3.3, 3.8, and 4.3 are 2.4 2.8, 3.2, 3.7, and 4.2.

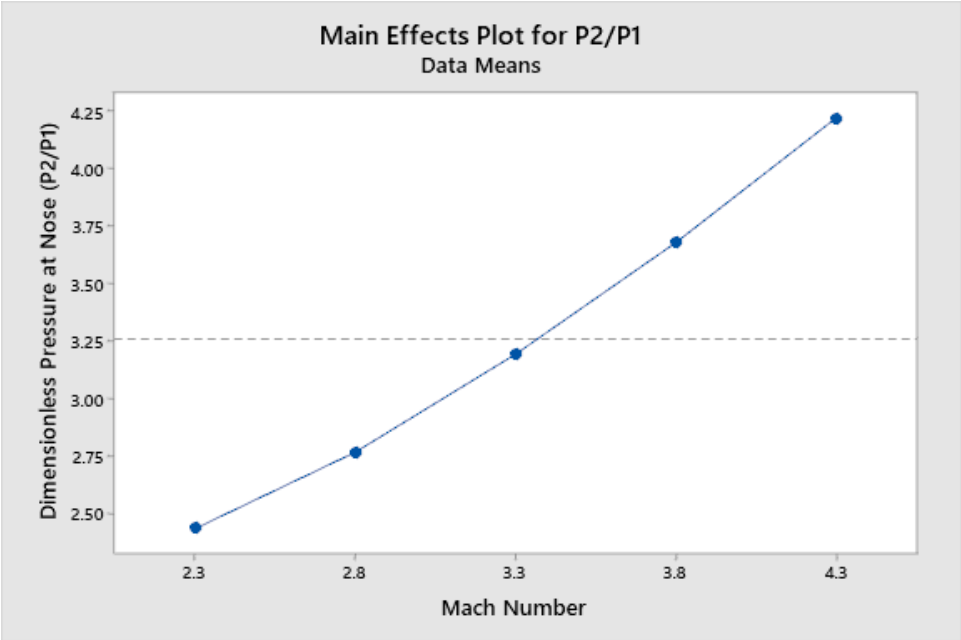

Fig. 5. illustrates the primary impact of Mach number on dimensionless static pressure (P2/P1)

3.2 Main effects plot for dimensionless static pressure

The major effect map for dimensionless static pressure at the wedge's nose is depicted in Figure 6. According to the data, as the wedge semi-vertex angle increases, so does the static pressure at the nose. With the progressive increase in the semi-vertex angle the surface area of the wedge increases. This increase in the surface area of the wedge will result in totally different pressure and hence the larger value of the pressure ratio. From Fig. 6 it is seen that when semi-vertex angle θ = 5, 10, 15, 20, and 25 degrees the corresponding surface pressure ratios are 1.5, 2.2, 3, 4.2, and 5.8. These results reiterate that the surface pressure ratio also increases with the increase in the semi-vertex angle of the wedge. The increase in the pressure ratio is almost linear.

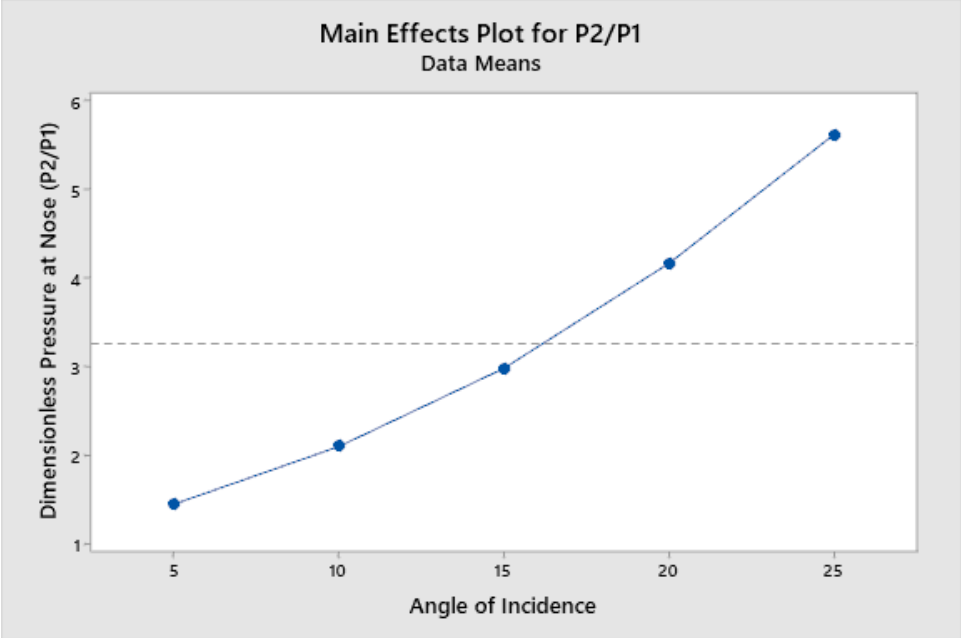

Fig. 6. illustrates the main impact of incidence angle on dimensionless static pressure (P2/P1)

3.3 The Pressure contour for static pressure

Analytical findings and CFD results are found to be in very excellent agreement. The analytical results and the CFD analysis results have a maximum divergence of 10%. In Fig. 7a-ac, which displays the static pressure contours for various Mach numbers and angles of incidence, it can be seen that as Mach increases, the strength of the oblique shock wave increases, and the magnitude of the Mach cone angle decreases. The base region grows as the wedge angle increases. It is also seen that the shock strength is high when the semi-vertex angle of the wedge is small and the Mach number is enhanced from the value of 1.3 to 1.8. However, when for fix Mach number whenever the wedge angle is increased it results in a weak shock wave.

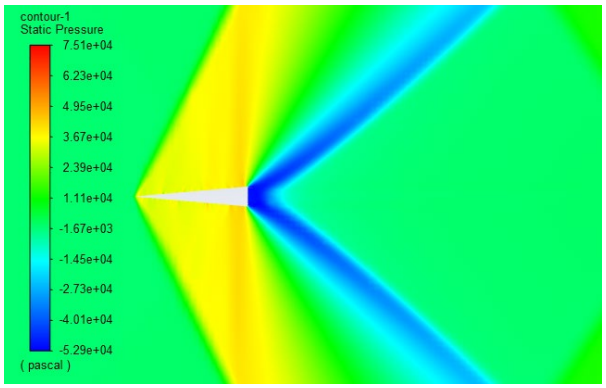

a) M=1.3 ,θ=5°

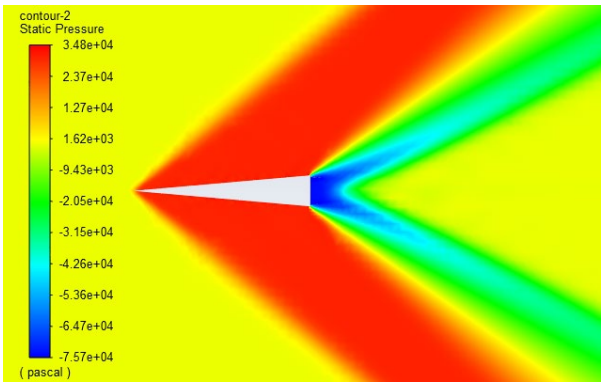

b) M=1.8 ,θ=5°

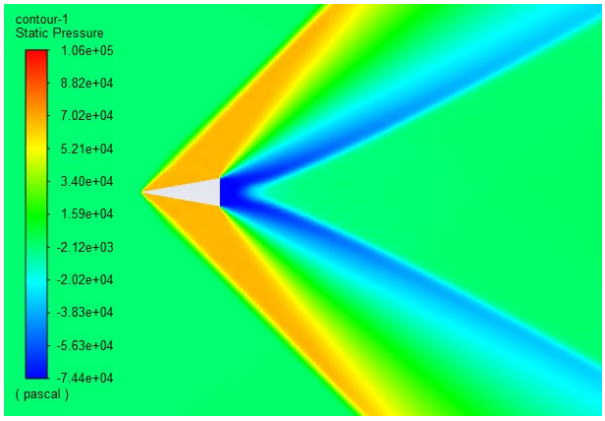

c) M=1.8 ,θ=10°

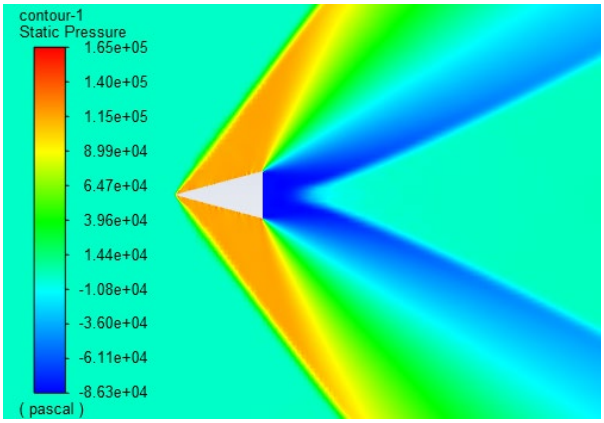

d) M=1.8 ,θ=15°

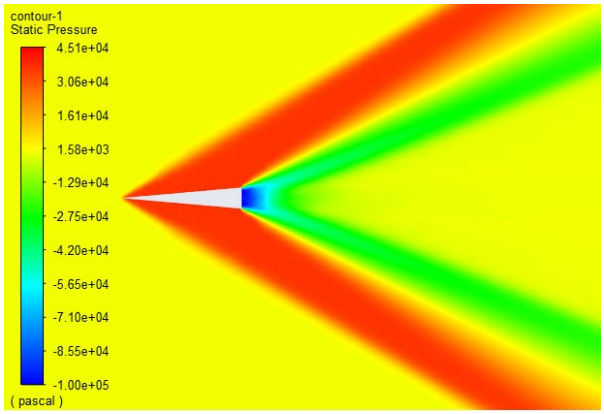

e) M=2.3 ,θ=5°

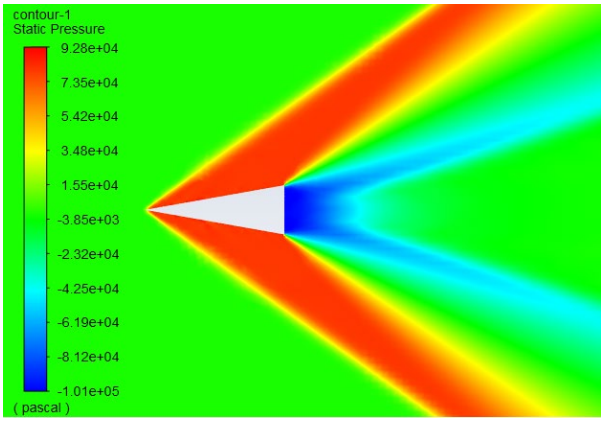

f) M=2.3 ,θ=10°

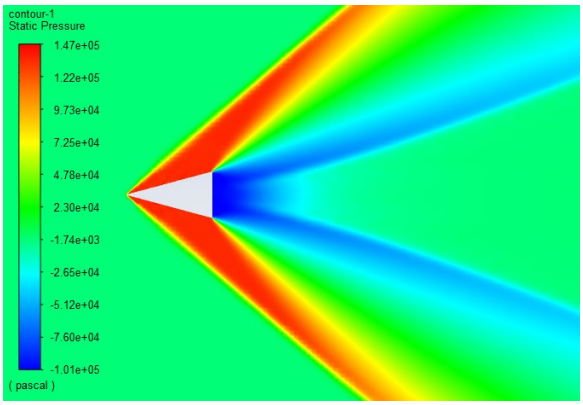

g) M=2.3 ,θ=15°

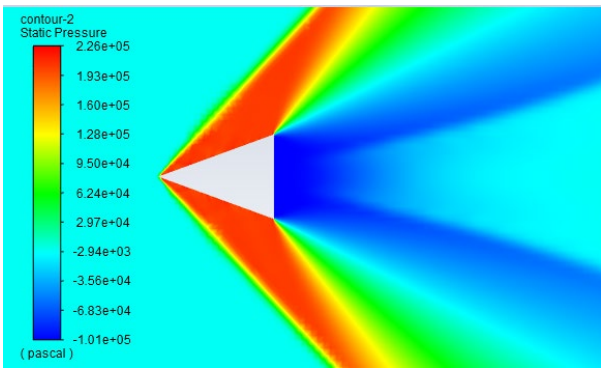

h) M=2.3 ,θ=20°

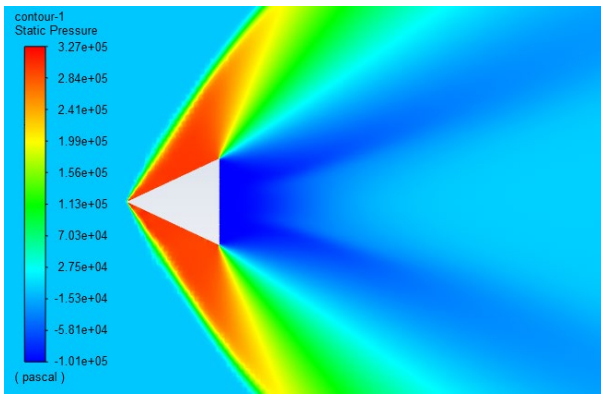

i) M=2.3 ,θ=25°

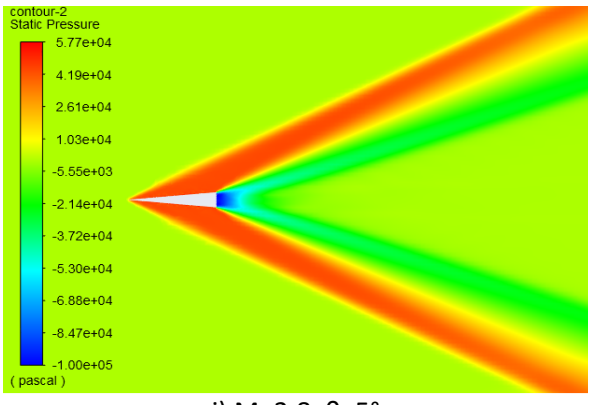

j) M=2.8 ,θ=5°

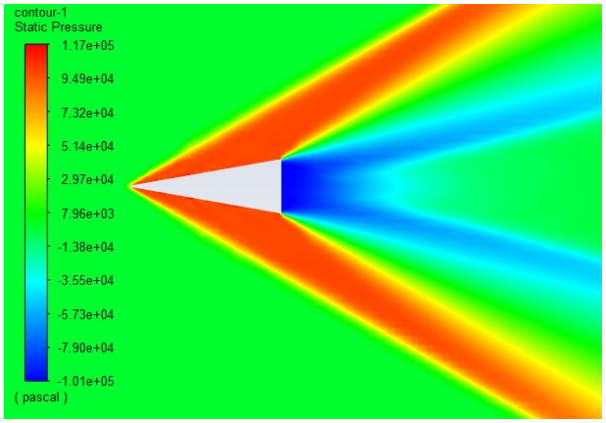

k) M=2.8 ,θ=10°

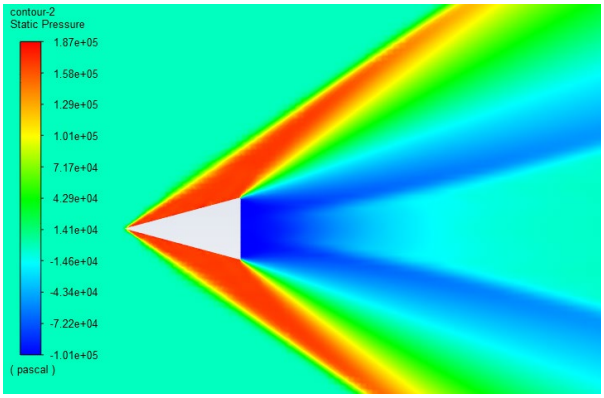

l) M=2.8 ,θ=15°

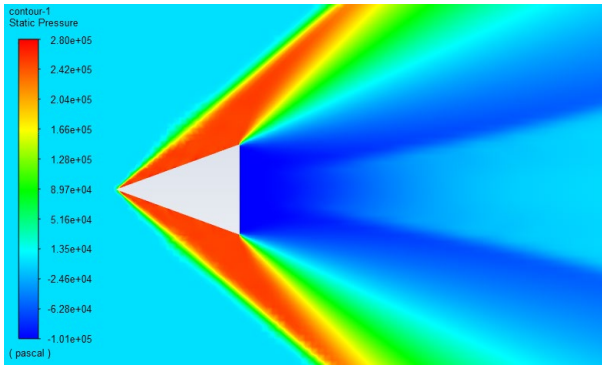

m) M=2.8 ,θ=20°

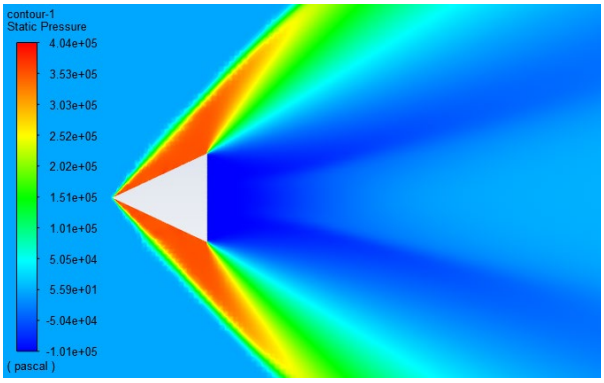

n) M=2.8 ,θ=25°

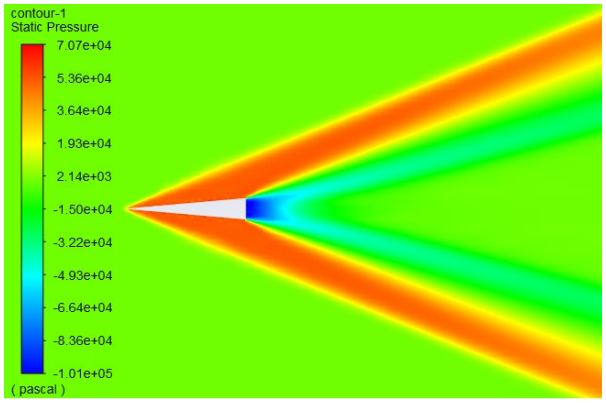

o) M=3.3 ,θ=5°

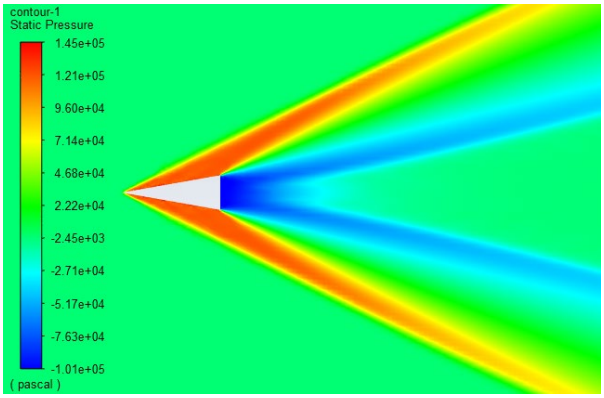

p) M=3.3 ,θ=10°

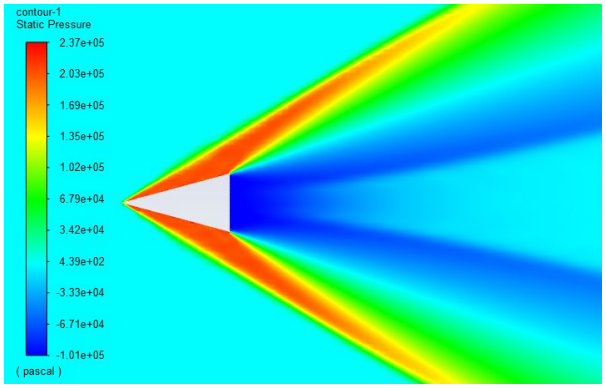

q) M=3.3 ,θ=15°

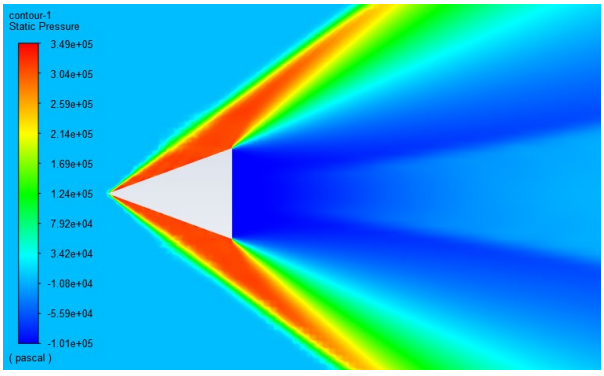

r) M=3.3 ,θ=20°

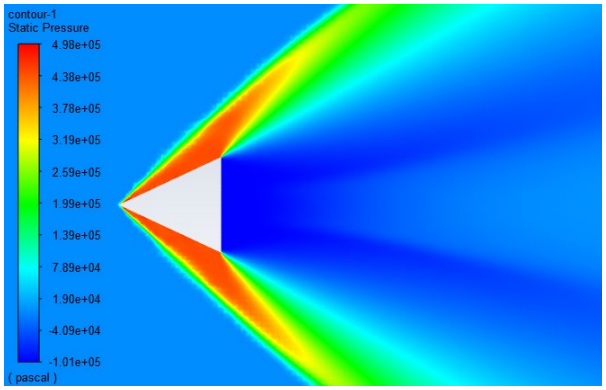

s) M=3.3 ,θ=25°

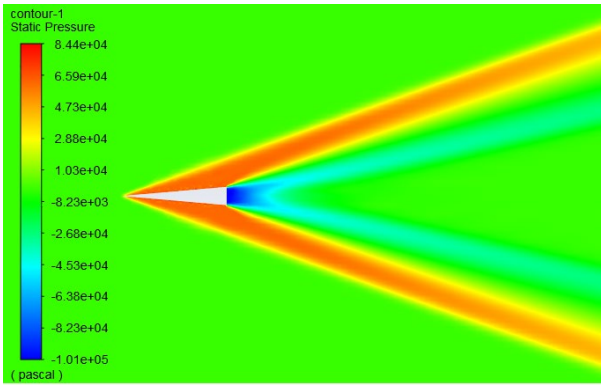

t) M=3.8 ,θ=5°

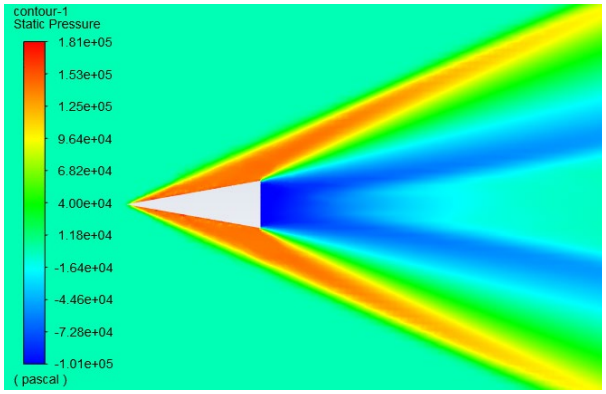

u) M=3.8 ,θ=10°

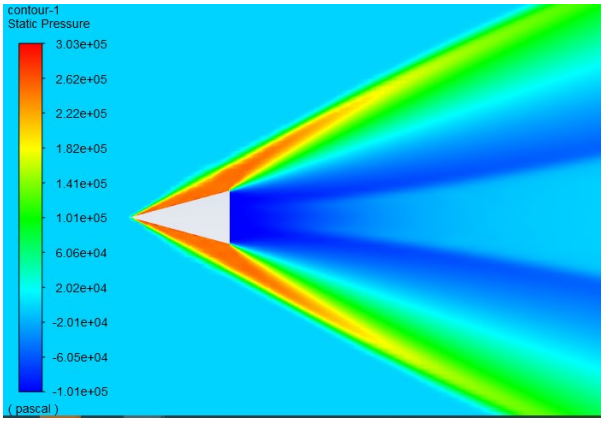

v) M=3.8 ,θ=15°

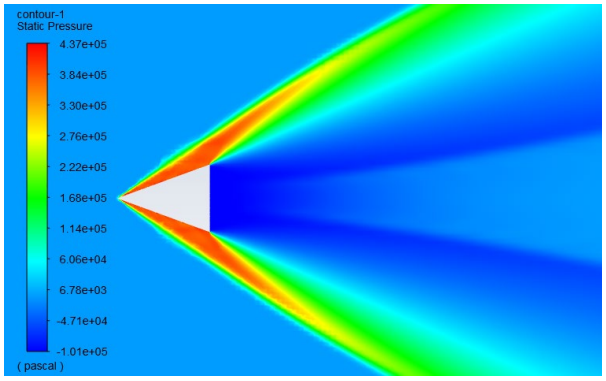

w) M=3.8 ,θ=20°

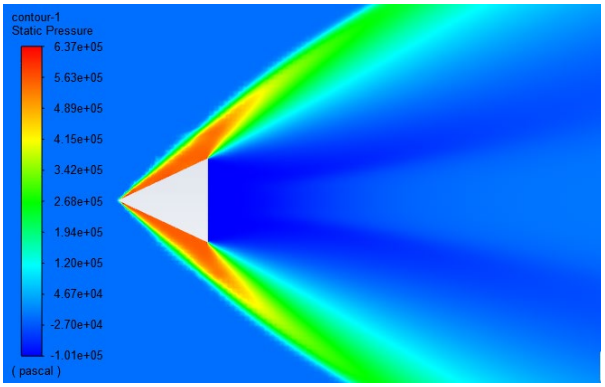

x) M=3.8 ,θ=25°

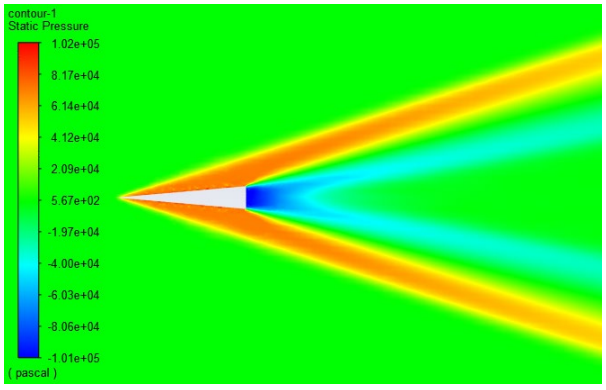

y) M=4.3 ,θ=5°

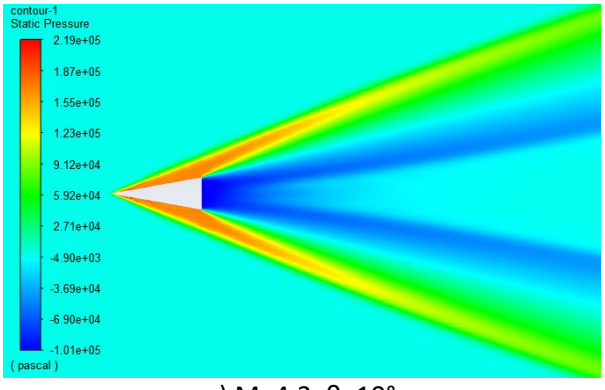

z) M=4.3 ,θ=10°

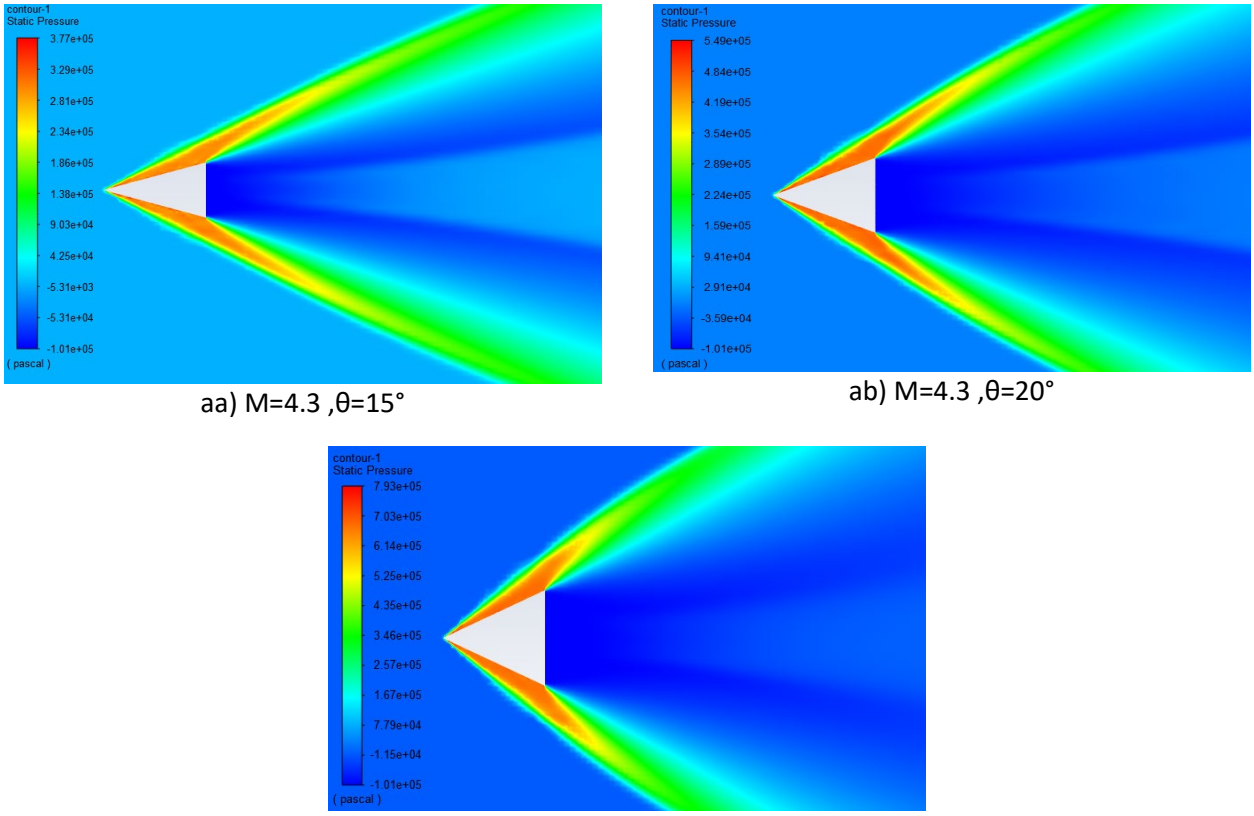

aa) M=4.3 ,θ=15°

ab) M=4.3 ,θ=20°

ac) M=4.3 ,θ=25°

Fig. 7. The static pressure contours for each scenario taken into account

3.4 The Effect of Mach number on pressure at the nose

The fluctuations of dimensionless static pressure at the Wedge's nose vs. Mach values for varied angles of incidences are depicted in Fig. 8a and Fig.8b, the acquired data make it abundantly evident that there is excellent agreement between the CFD and analytical results. The atmospheric pressure is used to split the absolute static pressure to create non-dimensionalized pressure. The dimensionless pressure rises as the Mach number rises. With an increase in Mach number from 1.3 to 4.3, the change in pressure at the nose is minimal at the lower wedge angles, i.e., θ = 5°and 10°. The effectiveness of the Mach number rises as the wedge angle does, and the change in pressure at the nose also rises significantly.

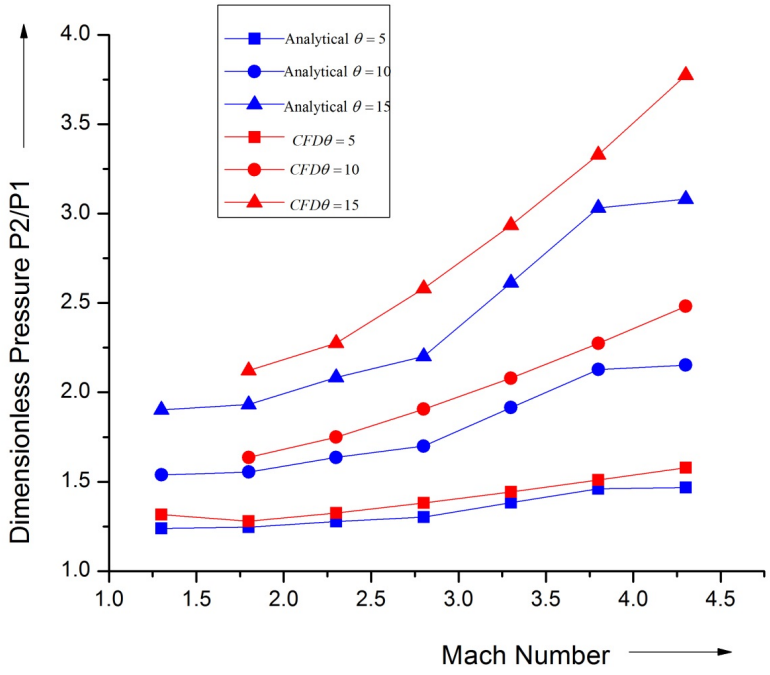

Fig. 8a. Mach number and variation in dimensionless pressure

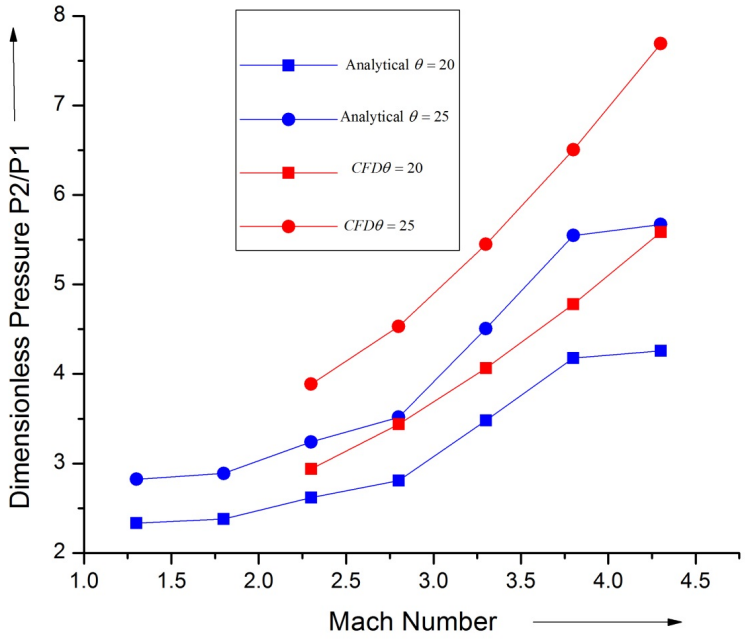

Fig. 8b. Mach number and variation in dimensionless pressure

3.5 The Effect of angle of incidence on pressure at the nose

The fluctuations in dimensionless static pressure at the wedge's nose versus wedge angle for different Mach numbers are depicted in Fig. 9a and Fig. 9b. Due to the increase in shock strength,

the static pressure at the nose rises with the wedge angle for all the Mach numbers. For wedge angles between θ = 5° and 10°, there is a slight increase in pressure for the supersonic Mach number.

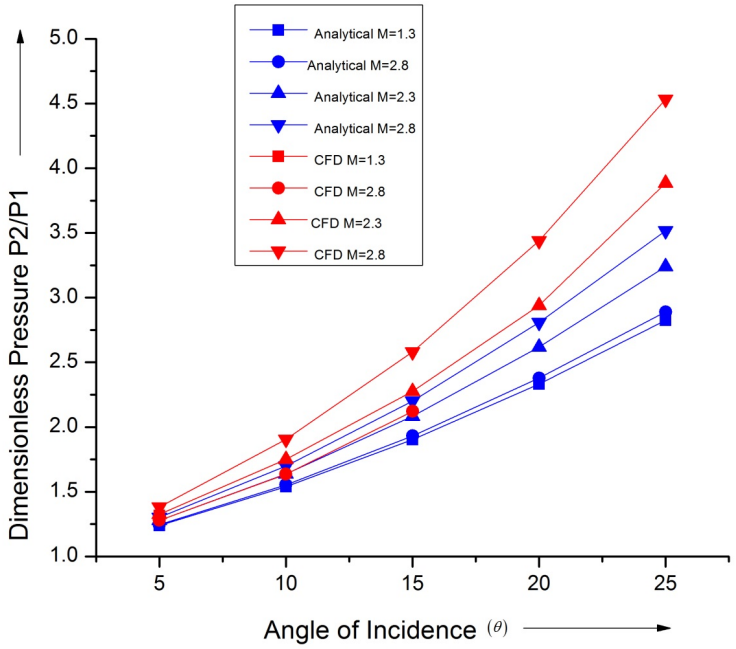

Fig. 9a. Dimensionless pressure Vs the angle of incidence

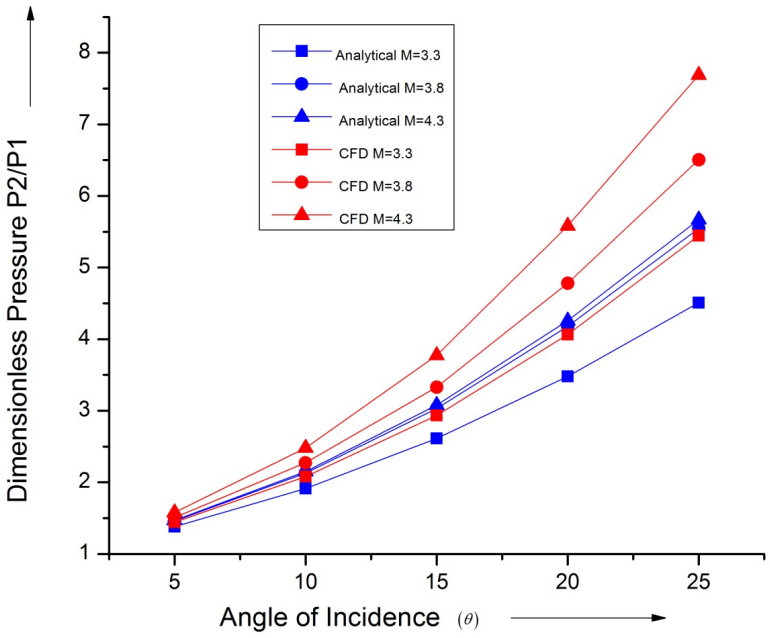

Fig. 9b. Dimensionless pressure Vs the angle of incidence

3.6 The Contour plot of dimensionless pressure at the nose

The contour plot for the pressure at the nose is shown in Figure 10. Based on the contour plot it can be observed that the pressure on the nose of the 2D wedge increases with an increase in Mach number as well as the angle of incidence. The pressure on the nose has a maximum value of larger than 7 times the atmospheric pressure at Mach number larger than 4 and an angle of incidence of close to 25 degrees.

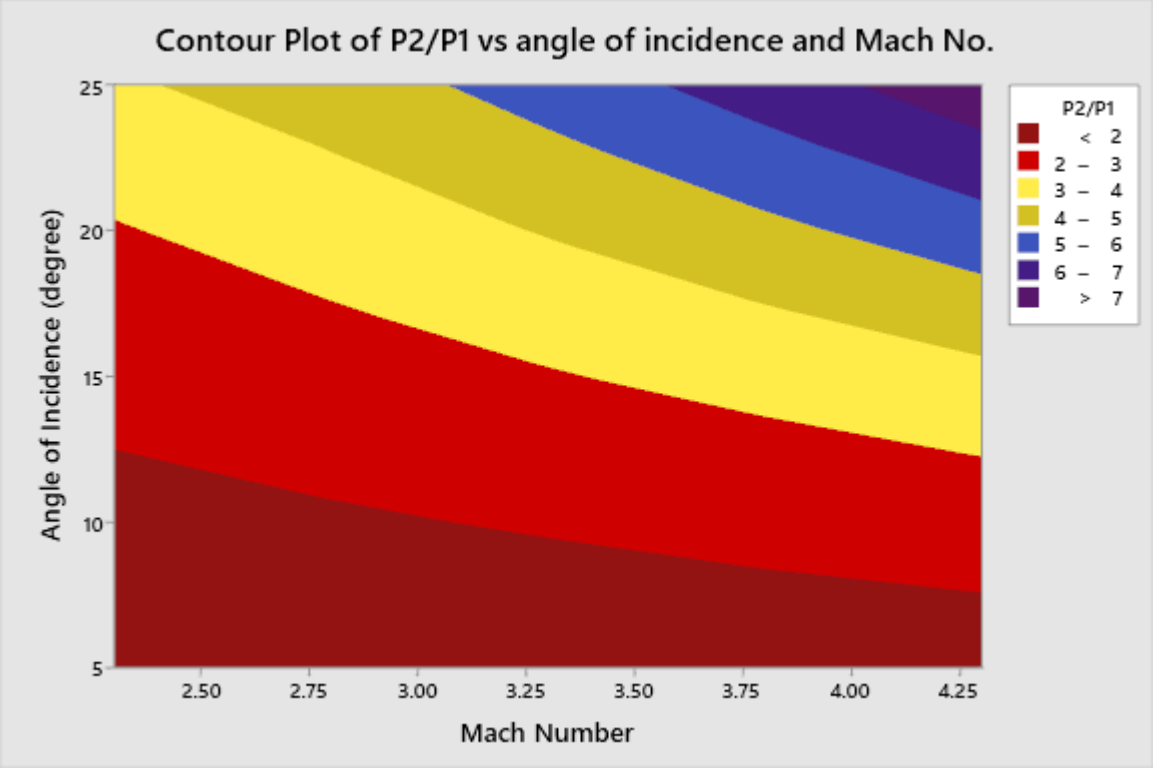

Fig. 10. Contour plot of dimensionless pressure at nose Vs Mach number and Angle of Incidence

4. Regression Analysis

Based on the results obtained by CFD analysis, the regression analysis is done by considering full factorial design. The total possible combinations of the parameters with their levels are considered to develop the regression equation.

4.1 Regression Equation

The regression equation is developed considering the main effects as well as interaction effects. The regression equation to predict the pressure value at the nose of the 2D wedge is shown in equation 6.

$$p_2/p_1 = \begin{bmatrix} 0.7 + 0.1896T - 0.029M - 0.00417T^2 + 0.127M^2 - 0.0976T \times M \\ + 0.000026T^3 - 0.0246M^3 + 0.002562T^2 \times M + 0.0169T \times M^2 \end{bmatrix} \quad (6)$$

4.2 Regression Equation Model Summary and Analysis of Variance

The summary of the regression equation (6) is shown in Table 2. Based on the summary it can be seen that the R square adjusted value and R square predicted value for the regression model are 99.97% and 99.89% respectively. Hence the regression equation shown in Eq. (6) can predict more accurate values of the pressure at the nose of the 2D wedge.

Table 2
Regression Equation Model Summary

S	R-sq	R-sq(adj)	R-sq(pred)
0.0303323	99.98%	99.97%	99.89%

The analysis of variance for the regression equation is shown in Table 3. Based on the fisher (F) values and P values for different combinations of parameters it can be concluded that the main parameters and their interactions have a significant role in the regression equation.

Table 3
Analysis of Variance

Source	DF	Adj SS	Adj MS	F-Value	P-Value
Regression	9	70.7982	7.86647	8550.06	0.000
T	1	0.0279	0.02787	30.30	0.000
M	1	0.0000	0.00000	0.00	0.975
T*T	1	0.0075	0.00750	8.15	0.012
M*M	1	0.0002	0.00018	0.20	0.662
T*M	1	0.0394	0.03942	42.84	0.000
T*T*T	1	0.0007	0.00074	0.80	0.385
M*M*M	1	0.0007	0.00068	0.74	0.403
T*T*M	1	0.1436	0.14361	156.09	0.000
T*M*M	1	0.0625	0.06246	67.89	0.000
Error	15	0.0138	0.00092		
Total	24	70.8120			

5. Conclusions

The pressure distribution is calculated analytically using the existing piston theory, and the results are then compared with those of the CFD study. The findings and CFD results are in perfect agreement with one another. It has been found that both the Mach number and the wedge angle have an impact on the variation of dimensionless pressure. It is also noted that the dimensionless static pressure at the wedge's only marginally varied for lower wedge angles and lower Mach values. These insights are valuable for designing aeronautical vehicles due to the expensive wind tunnel tests. As a result, these discoveries can be used to enhance aeronautical vehicle design during the initial development of missiles, rockets, bombs, and launch vehicles. The current investigation yields reliable results.

Acknowledgment
We gratefully thank the Management and Mangalore Institute of Technology and Engineering for their continuous support of my research work.

References

[1] Hui, W. H. "Supersonic and hypersonic flow with attached shock waves over delta wings." *Proc. Roy. Soc. London. A. Math.Phys. Sci.* 325, 1561, (1971): 251-268. https://doi.org/10.1098/rspa.1971.0168.

[2] Lui, D.D. and Hui, W.H. "Oscillating delta wings with attached shock waves.", *AIAA J.*, 15, no. 6, (1977): 804-812. https://doi.org/10.2514/3.7371.

[3] Lighthill, M. J. "Oscillating aerofoil at high Mach numbers." *J. Aeronaut. Sci.*, 20, no. 6, (1953): 402-406. https://doi.org/10.2514/8.2657.

[4] Ghosh, K. and Mistry, B. K. "Large incidence hypersonic similitude and oscillating non-planar wedges." *AIAAJ.*, 18, no. 8, (1980): 1004-1006. https://doi.org/10.2514/3.7702.

[5] Ghosh, K. "Hypersonic large deflection similitude for oscillating delta wings." *Aeronaut. J.* 88, (878), (1984): 357-361. https://doi.org/10.1017/S0001924000020868.

[6] Kalimuthu, R., Mehta, R.C. and Rathakrishnan, E. "Measured aerodynamic coefficients of without and with a spiked blunt body at Mach 6." *Adv. Aircraft Spacecraft Sci.* 6, no. 3, (2019): 225-238. https://doi.org/10.12989/aas.2019.6.3.225.

[7] Sher Afghan Khan, M A Fatepurwala, K N Pathan, P S Dabeer & Maughal Ahmed Ali Baig. "CFD Analysis of Human Powered Submarine to Minimize Drag." *International Journal of Mechanical and Production Engineering Research and Development (IJMPERD)* 8, no. 3 (2018): 1057-1066. https://doi.org/10.24247/ijmperdjun2018111

[8] Khan, S.A., Aabid, A. and Saleel, C.A. (2019), "CFD simulation with analytical and theoretical validation of different flow parameters for the wedge at supersonic Mach number." *Int. J. Mech. Mech. Eng.* 19, no. 1, (2019): https://www.researchgate.net/publication/331556786.

[9] Asha Crasta and S. A. Khan. "Hypersonic Similitude for Planar Wedges." *International Journal of Advanced Research in Engineering and Technology* 5, no. 2, (2014): 16-31. https://www.researchgate.net/publication/281192559

[10] Shaikh Javed, Kumar Krishna, Pathan Khizar, and Khan Sher. "Analytical and computational analysis of pressure at the nose of a 2D wedge in high-speed flow." *Advances in Aircraft and Spacecraft Science* 9, no. 2, (2022): 119-130. https://doi.org/10.12989/aas.2022.9.2.119

[11] Pathan K A, Khan S A, Shaikh A N, Pathan A A, and Khan S A. "An investigation of the boat-tail helmet to reduce drag." *Adv. Aircraft Spacecraft Sci.* 8, no. 1, (2021), 239- 250. https://doi.org/10.12989/aas.2021.8.3.239.

[12] Pathan Khizar Ahmed, Prakash S Dabeer, and Sher Afghan Khan. "Investigation of base pressure variations in internal and external suddenly expanded flows using CFD analysis." *CFD Letters* 11, no. 4 (2019): 32-40.

[13] Pathan Khizar Ahmed, Prakash S Dabeer, and Sher Afghan Khan. "Influence of expansion level on base pressure and reattachment length." *CFD Letters* 11, no. 5 (2019): 22-36.

[14] Pathan Khizar Ahmed, Syed Ashfaq, Prakash S Dabeer, and Sher Afgan Khan. "Analysis of parameters affecting thrust and base pressure in suddenly expanded flow from nozzle." *Journal of Advanced Research in Fluid Mechanics and Thermal Sciences* 64, no. 1 (2019): 1-18.

[15] Pathan Khizar Ahmed, S A Khan, and P S Dabeer. "An Investigation of Effect of Control Jets Location and Blowing Pressure Ratio to Control Base Pressure in Suddenly Expanded Flows." *Journal of Thermal Engineering* 6, no. 2 (2020): 15-23. https://doi.org/10.18186/thermal.726106

[16] Pathan, Khizar Ahmed, Prakash S Dabeer, and Sher Afghan Khan. "Effect of nozzle pressure ratio and control jet location to control base pressure in suddenly expanded flows." *Journal of Applied Fluid Mechanics* 12, no. 4 (2019): 1127-1135. https://doi.org/10.29252/jafm.13.02.30049

[17] Pathan, Khizar Ahmed, Prakash S Dabeer, and Sher Afghan Khan. "An investigation to control base pressure in suddenly expanded flows." *International Review of Aerospace Engineering (I. RE. AS. E)* 11, no. 4 (2018): 162-169. https://doi.org/10.15866/irease.v11i4.14675

[18] Pathan, Khizar Ahmed, Prakash S Dabeer, and Sher Afghan Khan. "Optimization of area ratio and thrust in suddenly expanded flow at supersonic Mach numbers." *Case studies in thermal engineering* 12, (2018): 696-700. https://doi.org/10.1016/j.csite.2018.09.006

[19] Pathan Khizar Ahmed, S A Khan, and P S Dabeer. "CFD analysis of the effect of flow and geometry parameters on thrust force created by flow from nozzle." *2nd International Conference for Convergence in Technology (I2CT)*, (2017): 1121-1125. https://doi.org/10.1109/I2CT.2017.8226302

[20] Pathan Khizar Ahmed, S A Khan, and P S Dabeer. "CFD analysis of the effect of area ratio on suddenly expanded flows." *2nd International Conference for Convergence in Technology (I2CT)*, (2017): 1192-1198. https://doi.org/10.1109/I2CT.2017.8226315

[21] Pathan Khizar Ahmed, P S Dabeer, and S A Khan. "CFD analysis of the effect of Mach number, area ratio, and nozzle pressure ratio on velocity for suddenly expanded flows." *2nd International Conference for Convergence in Technology (I2CT)*, (2017): 1104-1110. https://doi.org/10.1109/I2CT.2017.8226299

[22] Pathan, Khizar A, Prakash S Dabeer, and Sher A Khan. "Enlarge duct length optimization for suddenly expanded flows." *Advances in Aircraft and Spacecraft Science* 7, no. 3 (2020): 203-214. https://doi.org/10.12989/aas.2020.7.3.203.

[23] Shaikh S.K, Pathan K. A., Chaudhary Z. I., Marlpalle B. G., and Khan S. A., (2020), "An investigation of three-way catalytic converter for various inlet cone angles using CFD" *CFD Letters,* 12(9), pp. 76–90.

[24] Shaikh S.K, Pathan K. A., Chaudhary Z.I., and Khan S. A., (2020), "CFD analysis of an automobile catalytic converter to obtain flow uniformity and to minimize pressure drop across the monolith" *CFD Letters,* 12(9), pp. 116-128.